JGR Atmospheres

RESEARCH ARTICLE
10.1029/2023JD038722

The Lack of a QBO-MJO Connection in Climate Models With a Nudged Stratosphere

Zane K. Martin[1], Isla R. Simpson[2], Pu Lin[3], Clara Orbe[4], Qi Tang[5], Julie M. Caron[2], Chih-Chieh Chen[2], Hyemi Kim[6,7], L. Ruby Leung[8], Jadwiga H. Richter[2], and Shaocheng Xie[5]

[1]Department of Atmospheric Science, Colorado State University, Fort Collins, CO, USA, [2]Climate and Global Dynamics Laboratory, National Center for Atmospheric Research, Boulder, CO, USA, [3]Program in Atmospheric and Oceanic Science, Princeton University, Princeton, NJ, USA, [4]NASA Goddard Institute for Space Studies, New York, NY, USA, [5]Lawrence Livermore National Laboratory, Livermore, CA, USA, [6]Department of Science Education, Ewha Womans University, Seoul, Republic of Korea, [7]School of Marine and Atmospheric Sciences, Stony Brook, NY, USA, [8]Atmospheric Sciences and Global Change, Pacific Northwest National Laboratory, Richland, WA, USA

Key Points:

- The link between the quasi-biennial oscillation (QBO) and Madden-Julian oscillation (MJO) is explored in four climate models with nudged stratospheric winds and free-evolving tropospheres
- No model shows as strong of a QBO-MJO connection as in observations
- Model biases in cloud-radiative feedbacks and MJO vertical velocity are diagnosed, but neither conclusively explains the lack of a QBO-MJO connection

Correspondence to:
C. Orbe,
clara.orbe@nasa.gov

Citation:
Martin, Z. K., Simpson, I. R., Lin, P., Orbe, C., Tang, Q., Caron, J. M., et al. (2023). The lack of a QBO-MJO connection in climate models with a nudged stratosphere. *Journal of Geophysical Research: Atmospheres*, *128*, e2023JD038722. https://doi.org/10.1029/2023JD038722

Received 17 FEB 2023
Accepted 11 AUG 2023

Abstract The observed stratospheric quasi-biennial oscillation (QBO) and the tropospheric Madden-Julian oscillation (MJO) are strongly connected in boreal winter, with stronger MJO activity when lower-stratospheric winds are easterly. However, the current generation of climate models with internally generated representations of the QBO and MJO do not simulate the observed QBO-MJO connection, for reasons that remain unclear. This study builds on prior work exploring the QBO-MJO link in climate models whose stratospheric winds are relaxed toward reanalysis, reducing stratospheric biases in the model and imposing a realistic QBO. A series of ensemble experiments are performed using four state-of-the-art climate models capable of representing the MJO over the period 1980–2015, each with similar nudging in the stratosphere. In these four models, nudging leads to a good representation of QBO wind and temperature signals, however no model simulates the observed QBO-MJO relationship. Biases in MJO vertical structure and cloud-radiative feedbacks are investigated, but no conclusive model bias or mechanism is identified that explains the lack of a QBO-MJO connection.

Plain Language Summary Observations show a strong link between the stratospheric quasi-biennial oscillation (QBO)—the alternation of tropical stratospheric zonal winds between easterly and westerly phases—and the Madden-Julian oscillation (MJO), an eastward propagating phenomenon in the tropical troposphere in which the circulation and convection are coupled. Stronger MJO activity is observed when lower-stratospheric winds are easterly. This coupling is intriguing for many reasons, but most practically because it suggests that the stratosphere can potentially enhance surface weather and inform subseasonal climate prediction. However, current climate models do not show this observed connection. One reason may be related to biases in how models simulate stratospheric winds, which can be corrected for in an artificial way by relaxing the model simulated winds to better match observationally constrained data sets. One recent study, however, showed that correcting for this bias using this approach in one climate model still fails to produce credible QBO-MJO coupling. Here we expand that analysis to include four climate models and find that no model produces a robust QBO-MJO relationship like that seen in observations. Our results show that properly representing the QBO winds and temperatures via nudging is therefore not sufficient for reproducing the observed relationship. Furthermore, while biases in how models represent cloud processes may still be a likely culprit, any definitive model bias or missing mechanism remains elusive.

1. Introduction

The quasi-biennial oscillation (QBO; Baldwin et al., 2001; Ebdon, 1960; Reed et al., 1961)—a descending, ~28 months reversal in the tropical stratospheric zonal wind—is the most significant mode of interannual variability in the tropical stratosphere. While QBO signals are strongest in the tropical stratosphere, through teleconnections the QBO modulates climate processes outside the tropics and below the stratosphere (Anstey et al., 2022 Camargo & Sobel, 2010 Garfinkel & Hartmann, 2011; Gray et al., 2018; Holton & Tan, 1980). In particular, a strong connection has recently been observed between the QBO and the Madden-Julian oscillation (MJO; Madden & Julian, 1971, 1972), a subseasonal, eastward propagating envelope with strong coupling of tropical convection and circulation. During boreal winter, MJO activity and strength is significantly enhanced when the QBO is in the easterly phase relative to the westerly phase (Martin, Son, et al., 2021; Son et al., 2017;

Yoo & Son, 2016). This QBO-MJO connection modulates MJO predictability and its teleconnections (Feng & Lin, 2019; Kim et al., 2019; Lim et al., 2019; Marshall et al., 2017; Mayer & Barnes, 2020; Toms et al., 2020; Wang et al., 2018, 2019). Yet despite these far-reaching impacts, the QBO-MJO connection remains theoretically difficult to explain (Martin, Son, et al., 2021).

Challenges in understanding the physics behind the QBO-MJO connection are in large part hampered by the inability of climate models to capture the connection. While convection-permitting models (Back et al., 2020; Martin et al., 2019) and subseasonal forecast models (Abhik & Hendon, 2019; Martin et al., 2020) have shown some indication of a QBO-MJO link, model signals in both frameworks are weaker-than-observed and difficult to confidently detect or interpret. Free-running global climate models (GCMs) present an alternative framework in which to examine this problem, which is attractive given that many GCMs are now capable of internally simulating both a QBO and an MJO (e.g., Ahn et al., 2020; Kim et al., 2020; Richter et al., 2020; Orbe, Van Roekel, et al., 2020). However, GCMs have repeatedly failed to show any QBO-MJO link (Kim et al., 2020 Lee & Klingaman, 2018; Lim & Son, 2020; Martin, Orbe, et al., 2021).

A frequent hypothesis for why climate models do not capture a QBO-MJO connection are biases in the model stratosphere, in particular the QBO representation in the lower stratosphere and the tropical tropopause layer (TTL) (Kim et al., 2020; Lee & Klingaman, 2018; Lim & Son, 2020; Martin et al., 2019; Martin, Son, et al., 2021). Most state-of-the-art climate models show weaker-than-observed QBO variability in the TTL, in particular in QBO temperature signals. These biases might be important, as QBO temperature anomalies and their effect on upper tropospheric static stability are a proposed mechanism for the QBO-MJO connection (Martin, Son, et al., 2021). A straightforward way to test the hypothesis that stratospheric biases in models explain the lack of a QBO-MJO link is to impose the stratosphere in the model by "nudging" (e.g., Douville, 2009; Ferranti et al., 1990; Hitchcock & Simpson, 2014; Jeuken et al., 1996). This is done by adding artificial tendency terms that relax the model toward a target profile such as reanalysis (e.g., Jeuken et al., 1996). In the context of the QBO-MJO link, Martin, Orbe, et al. (2021) (herein M21) carried out a nudged climate model experiment in which the global stratospheric meridional and zonal winds were relaxed toward reanalysis while the troposphere was not nudged. M21 showed that while QBO winds and temperatures were captured successfully in the nudged model, no QBO-MJO link was evident across an ensemble of simulations.

Here, we extend the work in M21 by repeating a similar stratospheric nudging experiment across four state-of-the-art climate models, each with several ensemble members run from 1980 to 2014. The use of multiple models allows us to explore the degree to which the findings in M21 were model specific, and to increase confidence that the results of that study were robust. Further, they allow us to explore whether models share any common biases important to the QBO-MJO link.

In Section 2, we present more details regarding the four GCMs and the stratospheric nudging experimental design, as well as other data sets and methodology. Section 3 diagnoses the nudged models' representation of the QBO (Section 3.1), the MJO (Section 3.2), and the QBO-MJO connection (Section 3.3). Section 4 summarizes our findings.

2. Data and Methods

2.1. Climate Models and Nudging Experimental Design

Simulations were conducted using four atm-ocean coupled climate models: the Community Earth System Model, version 2 (referred to here as CESM, Danabasoglu et al., 2020); the Energy Exascale Earth System Model version 1 (referred to here as E3SM, Golaz et al., 2019); the Geophysical Fluid Dynamics Laboratory CM4 (referred to here as GFDL, Held et al., 2019); and the NASA Goddard Institute for Space Studies Model E2.1-G (referred to here as GISS, Kelley et al., 2020).

In each of the four models, a three-member ensemble of simulations was conducted over the historical period from 1 January 1980 to 31 December 2014 with the CMIP6 historical forcings (Eyring et al., 2016). In each simulation, the model stratospheric zonal and meridional wind were nudged toward time-varying reanalysis fields over the same time period. CESM, GFDL, and GISS were nudged to NASA's Modern-Era Retrospective Analysis for Research and Applications 2 (MERRA-2; Gelaro et al., 2017) reanalysis, while E3SM was nudged to ERA-Interim reanalysis (ERA-I; Dee et al., 2011) due to data availability for nudging in that model. The nudging

relaxation timescale in all models was set to 12 hr, and nudging was only implemented above 150 hPa. To smooth the transition from the nudged stratosphere to the nonnudged troposphere, the nudging timescales varied linearly from 150 to 100 hPa, with full-strength nudging above 100 hPa, and no nudging below 150 hPa. Nudging was implemented globally at all latitudes and was identically implemented in each ensemble member of a given model.

Nudging can be applied in several ways (see M21); we explore two strategies here. One option is to implement nudging such that the full 3D spatial structure of the model is nudged toward the 3D reanalysis at each grid point ("grid-point nudging"). An alternative approach is to nudge only the zonal-mean of model variables to match the zonal-mean of reanalysis ("zonal-mean nudging," Hitchcock & Simpson, 2014; Simpson et al., 2011). Note the latter case is not the same as nudging the model at each grid point to the zonal-mean: zonal asymmetries are allowed to exist in the zonal-mean nudged models. M21 found their overall results were insensitive to which nudging implementation was used, and zonal-mean nudging can be technically difficult to implement in certain model frameworks, especially those with unstructured grids. As such, both approaches were explored in this study. The CESM and GISS models used zonal-mean nudging, whereas the GFDL and E3SM models used grid-point nudging.

2.2. Other Data Sets and Methodology

Model performance is compared to observational and reanalysis products. In addition to MERRA-2 reanalysis, observed outgoing long-wave radiation (OLR) from the NOAA Interpolated OLR data set (Liebmann & Smith, 1996), observed precipitation from the Tropical Rainfall Measuring Mission (TRMM; Liu et al., 2012 version 7 Level 3 daily TRMM-3B42 data), and some additional meteorological variables from ERA-5 reanalysis (Hersbach et al., 2020) are used.

MJO indices are a common and useful way to summarize MJO characteristics. We use the Real-time Multivariate MJO index (RMM; Wheeler & Hendon, 2004) here. RMM is based on an empirical orthogonal function (EOF) analysis of tropical OLR and zonal winds at 200 and 850 hPa. The observed MJO index used is available from the Australian Bureau of Meteorology (see Data Availability Statement), while for the model simulations the RMM index is calculated following Wheeler and Hendon (2004), except that the model data are projected onto the observed rather than the model EOFs. This facilitates a fair comparison across models and between models and observations. The OLR-based MJO Index (OMI; Kiladis et al., 2014) was also explored, but as overall results discussed below were not sensitive to the choice of index (as was also found in M21) we present only results using RMM here.

We define the QBO phase using the monthly 50 hPa tropical zonal winds (e.g., Martin, Son, et al., 2021; Son et al., 2017; Yoo & Son, 2016), averaged zonally and from 10°N to 10°S (U50). QBO easterly months are defined when U50 is less than the mean minus half a standard deviation (QBOE) and QBO westerly months are defined when U50 is greater than the mean plus half a standard deviation (QBOW).

We further diagnose the representation of the stratospheric transformed Eulerian mean (TEM) vertical velocity. Due to data availability, ERA5 reanalysis was used to calculate TEM quantities for comparison to the four model simulations. Model TEM quantities were calculated following the DynVarMIP protocol (Gerber & Manzini, 2016).

3. Results

3.1. Nudged QBO and Stratospheric Representation

Nudging the model stratosphere leads to an accurate representation of the QBO signal across all four models, consistent with the strong nudging timescales and with results in M21. Figure 1 shows the time series of tropical-mean zonal-mean wind in MERRA-2 reanalysis and the first ensemble member of each model: the descending alternating easterly and westerly phases of the QBO are robustly captured in all models with nudging and match the reanalysis. Furthermore, despite the fact that temperature is not nudged in any model, QBO temperature signals are represented with fidelity down into the upper troposphere. For example, composites of QBO differences (QBOE minus QBOW) in temperature in reanalysis and each model shown in the right panels of Figure 1 indicate that the structure and magnitude of these temperature signals in the upper troposphere and

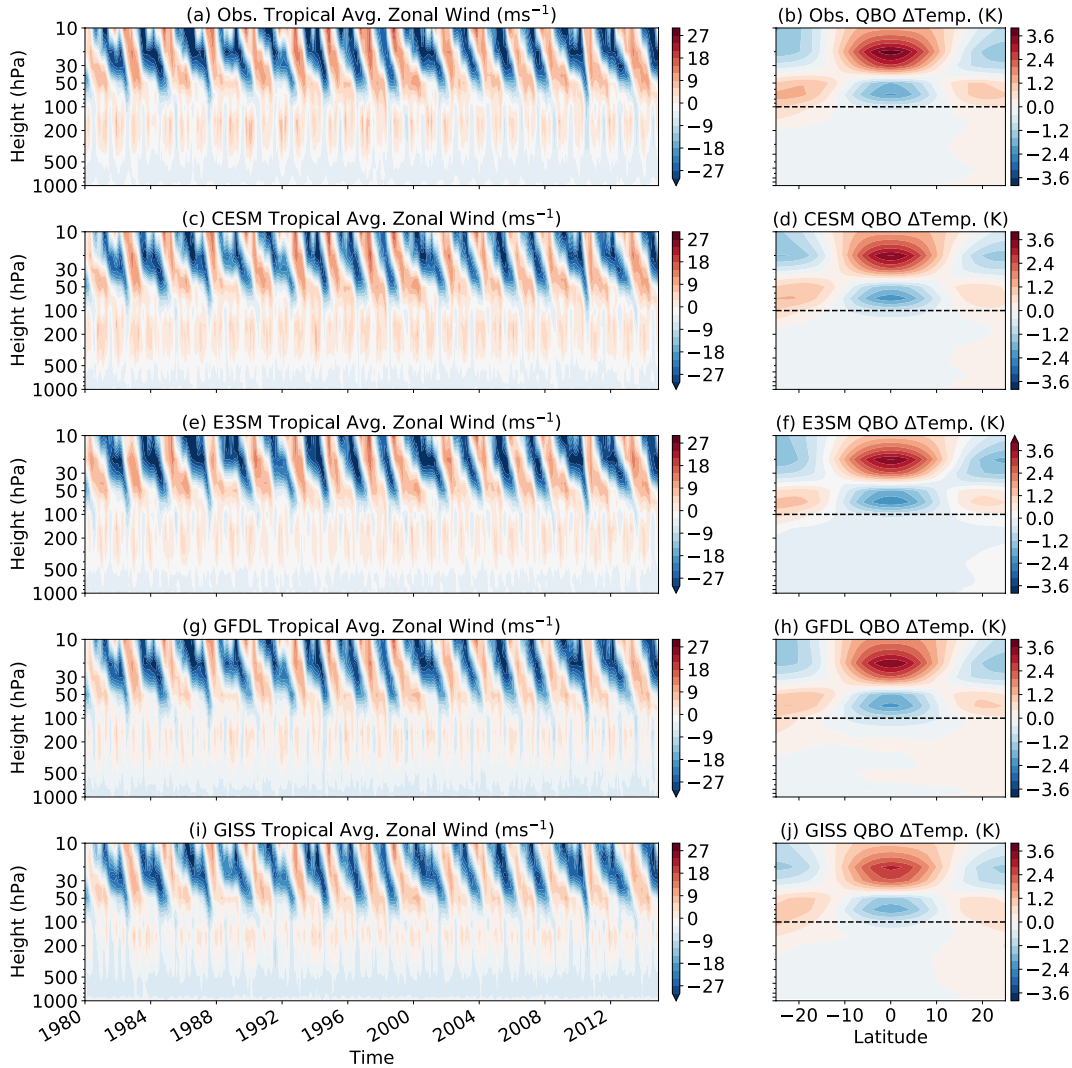

Figure 1. Left panels: The tropical-mean (zonal-mean averaged from 10°N to 10°S) zonal wind in Modern-Era Retrospective Analysis for Research and Applications 2 (MERRA-2) (a) and the four nudged climate simulations (c, e, g, and i). Right panels: The QBOE minus QBOW zonal-mean temperature in reanalysis (b) and the nudged models (d, f, h, and j). The dashed black line indicates the level above which nudging is applied.

lower stratosphere are successfully represented in the models with nudging. Overall, little variation in the QBO temperature signals is evident across models, again consistent with the fact that the zonal-mean winds in all models is strictly nudged toward reanalysis and temperatures adapt to be in balance with these nudged winds.

The seasonal cycle and deseasonalized time series of U50 further indicates how closely the models match the reanalysis of the zonal winds. Overall, the seasonal cycle of U50 in the reanalysis is generally well captured by the models (Figure 2a). Deseasonalized time series of U50 also show good agreement between reanalysis values and the CESM, GFDL, and GISS values (Figure 2b). Slight differences are evident in E3SM, due to the different reanalysis used as a target in this model (ERA-I); we confirmed that E3SM closely matches the ERA-I U50 (not shown). The seasonal cycle of temperature (Figure 2c) and deseasonalized temperature anomalies (Figure 2d) at 100 hPa averaged over the tropics (10°S to 10°N) are also shown; here there is more variability both between models and within the ensemble. The GFDL and GISS models feature annual cycles that are biased warm, relative to reanalysis values—the GISS model especially so in winter, whereas GFDL shows a warm bias in most months regardless of season. CESM, by comparison, most closely matches the observations, with only a slight warm bias.

E3SM shows more distinct 100 hPa temperature interannual signals than other simulations (Figure 2d). While still generally agreeing well with MERRA2, the E3SM model has a notable cold bias in the first decade of

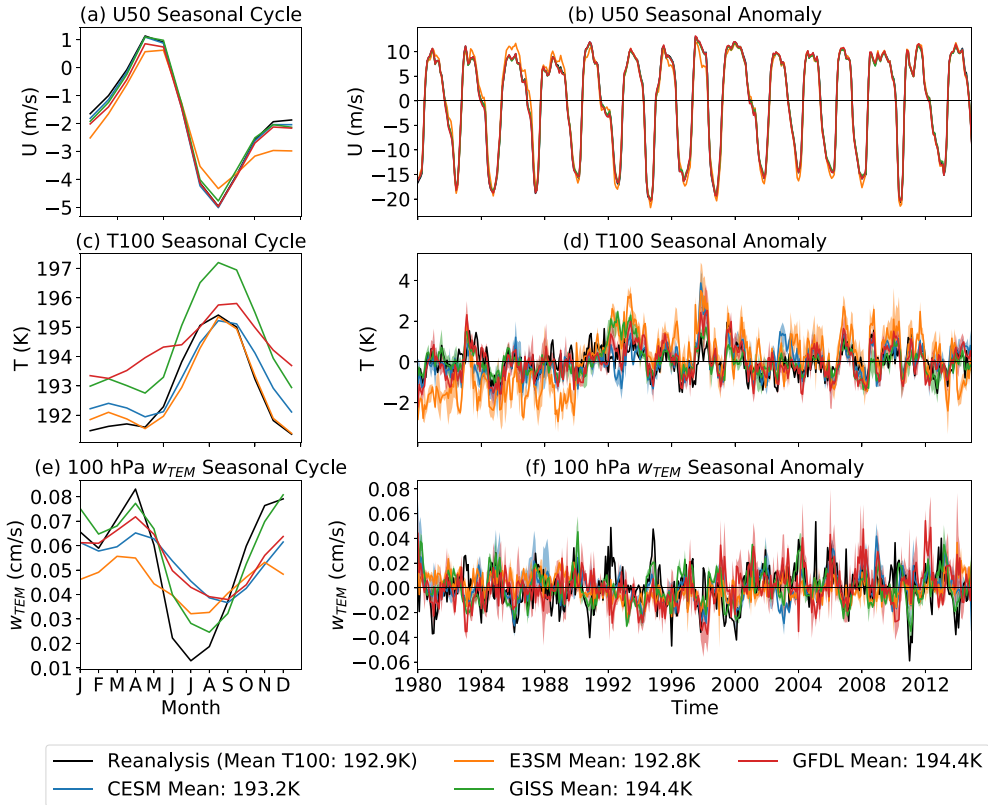

Figure 2. The 10°N/°S, all longitude-mean seasonal cycles (left panels) and monthly anomalies relative to the seasonal cycle (right panels) for several stratospheric variables. Panels (a/b) show 50 hPa zonal wind, panels (c/d) show 100 hPa temperature, and panels (e/f) show w_{TEM} vertical velocity at 100 hPa. Shading in the right panels shows the range across the ensemble of each model. The legend indicates the model, as well as the all-time mean 100 hPa temperature.

the simulation, after which it appears more comparable to other models. This may be in part due to the different reanalysis data set used to nudge the model: while temperature is not nudged, through the thermal wind constraint we expect the specific structure of the nudged zonal winds to influence temperature. ERA-I has colder winter temperatures than MERRA-2 during this decade (not shown), but even compared to ERA-I temperatures, E3SM is still biased cold during this period, especially during summers. Another distinct feature of E3SM which might in part explain the increased variability in TTL temperatures is the interactive ozone scheme (Hsu & Prather, 2009; Tang et al., 2011) used in E3SM; other models use specified ozone profiles. The prognostic stratospheric ozone concentration in E3SM varies with local temperature, which in turn modifies temperature by changing solar heating. It is possible that such ozone feedbacks might contribute to the stronger E3SM model biases, though this was not explored in detail and remains speculative.

While the nudging experiments are designed to ensure the meridional and zonal stratospheric winds associated with the QBO are well captured, stratospheric biases in other variables are not necessarily constrained. In particular, nudging experiments like those reported here do not ensure that the divergent component of the circulation is strictly enforced (Davis et al., 2022 DeWeaver & Nigam, 1997; Hitchcock & Haynes, 2014). More comprehensive (i.e., three-dimensional, full domain) nudging experiments can also exhibit large differences in the Transformed Eulerian Mean (TEM, Andrews et al., 1987) circulation compared to that of the target state, as was illustrated for models participating in the Chemistry Climate Modeling Initiative (Chrysanthou et al., 2019; Orbe, Plummer, et al., 2020). Indeed, Figure 2f, which shows time series of 100 hPa residual vertical velocity (w_{TEM}) demonstrates that while there are some similarities between the reanalysis and the nudged simulations, this field is not particularly well constrained by the nudging and generally exhibits lower variability than the reanalysis, especially in the GFDL model. Note that the seasonal cycle of w_{TEM} is also poorly constrained in the models (Figure 2e).

While the TEM circulation has not been theorized as central to the QBO-MJO link, we still feel this point important to note and highlight the degree to which nudging does not constrain all aspects of the QBO-associated

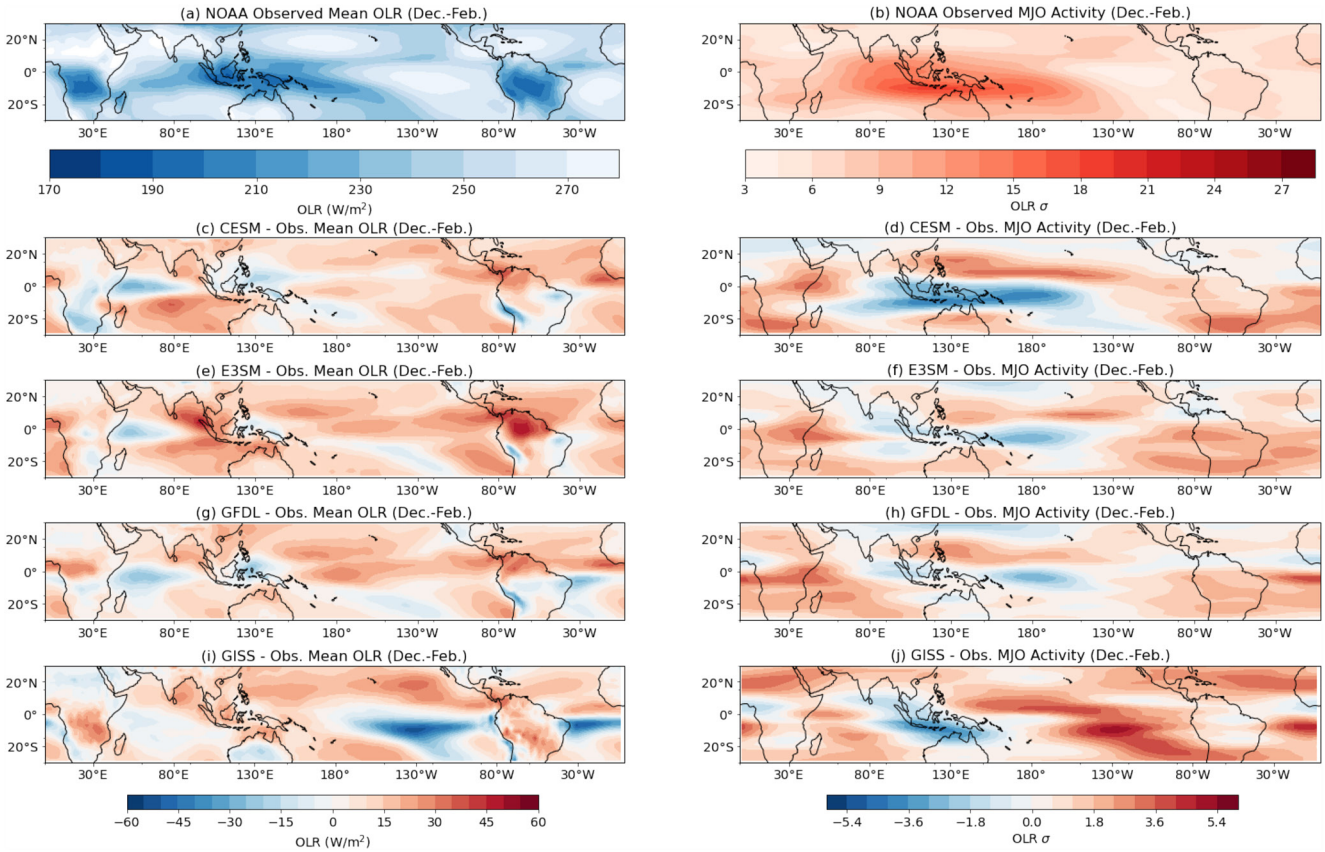

Figure 3. The observed December-February mean long-wave radiation (OLR) (a) and standard deviation of 20–100 days, eastward wavenumber 1–5, bandpass-filtered long-wave radiation (OLR) (b). Bottom panels (c–j) show differences between each model (interpolated onto the observed grid) and observations in both quantities.

circulation anomalies. We highlight this issue with nudging in general, and also note this aspect of model bias as a theoretical or observational avenue that future work on the QBO-MJO link might explore.

3.2. MJO Representation

The models' tropospheres are not nudged, such that MJO performance across the four models is not constrained by observations. Nevertheless, models whose representations of the MJO are reasonable were prioritized in this intercomparison, and the four models considered show MJO signals that represent relatively state-of-the-art capability in simulating the MJO (Danabasoglu et al., 2020; Kim et al., 2022; Zhao et al., 2018). Figure 3 shows the observed December-February (DJF) mean OLR (Figure 3a) and standard deviation of 20–100-day bandpass-filtered, eastward wavenumber 1–5 filtered, DJF OLR (Figure 3b). The latter is often used as a metric for MJO convective activity (e.g., Yoo and Son (2016)). Also shown are the model differences from observations (Figures 3c–3j) for one ensemble member; differences in these diagnostics across ensemble members are small and thus not shown. Overall, all models capture the overall distribution of winter-time convection with reasonable fidelity. A common feature in models is slightly too-low OLR over the western Indian ocean and too-strong in the subtropics. The GISS model also shows a prominent region of negative OLR bias over the eastern and central Pacific, which we hypothesize may be due to an overly active El Niño (Kelley et al., 2020), and which is not a feature other models demonstrate.

Models also show biases in MJO activity, though systematic biases across all models are not readily evident. Two models—CESM and GISS—show too weak MJO activity in the region of the Maritime Continent. In CESM, this is accompanied by increased winter-time MJO activity to the north of the Maritime Continent (Figure 3d), which may indicate the MJO in this model does not detour south of the Maritime Continent to the same extent as observed. In the GISS model, stronger-than-observed MJO activity is evident in the same eastern and central

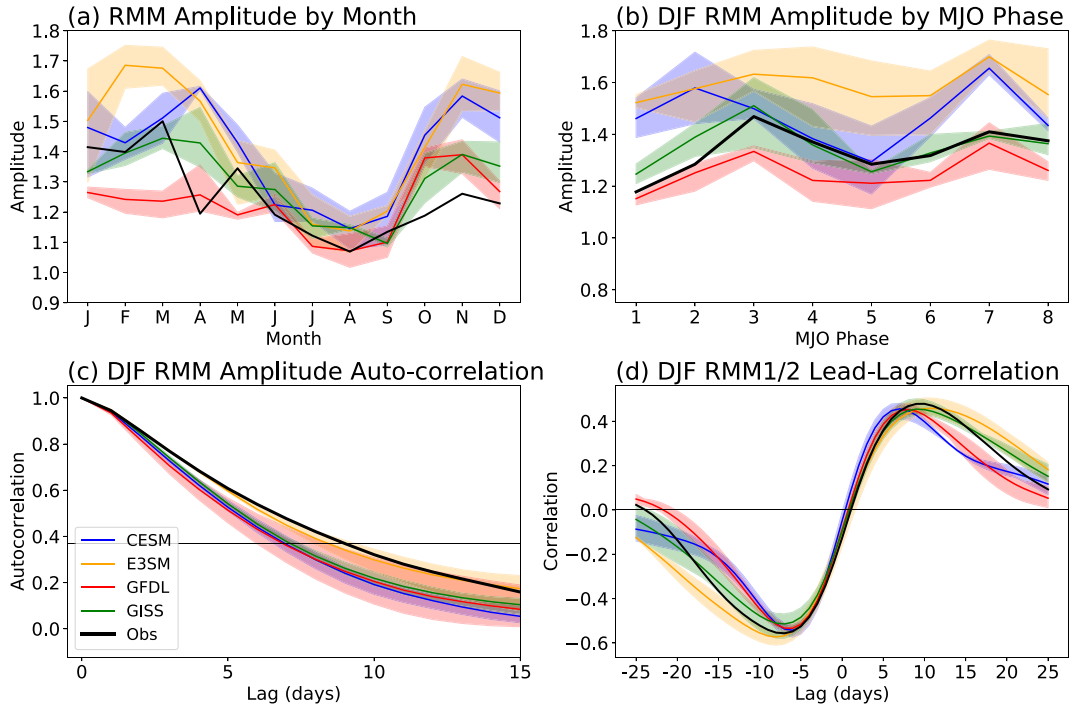

Figure 4. Real-time Multivariate Madden-Julian oscillation index (RMM) properties for observations and each model, with shading showing the ensemble spread. Panels show (a) the RMM amplitude binned by month; (b) the RMM amplitude binned by MJO phase; (c) the lagged autocorrelation in RMM amplitude as a function of day; and (d) the lead-lag correlation between RMM1 and RMM2 as a function of day.

Pacific region where mean OLR biases are prominent, possibly due to an extension of convective activities east of the MJO in this model due to the increased ENSO activity. Smaller biases around the Maritime continent are evident in GFDL or E3SM; both show slightly less MJO activity, but are generally comparable to observations.

Another way of measuring MJO activity and fidelity is through MJO indices—Figure 4 shows several metrics of how the RMM index in the models compares with observations. All models capture something akin to the observed seasonal cycle in RMM amplitude, with higher values in boreal winter and lower values in boreal summer (Figure 4a), though a range of seasonal cycle behavior is still evident. Models tend to overestimate MJO activity in late fall and early winter, with the GISS and CESM models looking closest to observations during the rest of the year. The GFDL model shows weaker amplitude in general during January-March, whereas E3SM shows stronger MJO amplitude during this period in particular, as well as at other points during the year. During DJF, the season when the observed QBO-MJO link is evident, models show a range of RMM amplitudes. Sensitivity of RMM amplitudes to the MJO phase is not large (Figure 4b) in models or observations, though the behavior discussed above is evident with the GFDL model having slightly weaker than observed amplitude, CESM and GISS being closer to observed, and E3SM showing stronger-than-observed behavior throughout all MJO phases.

Note that the RMM results are somewhat in contrast with the weaker-than-observed signals in MJO activity in certain models, like CESM, seen in Figure 3. We attribute this difference to several aspects: MJO activity, defined in Figure 3 using bandpass-filtered OLR, measures the local subseasonal convective variability at each grid point, whereas RMM measures the global signal of the MJO across convection and circulation, with circulation signals being more dominant drivers of RMM (Straub, 2013; Ventrice et al., 2013). Biases in particular regions and variables—like convective activity over the Maritime Continent—may be offset by global wind and convective signals viewed through RMM. Composite plots of bandpass-filtered OLR onto the RMM phase further confirmed that OLR signals around the Maritime Continent were weaker than observed (not shown).

Figure 4 also shows the lagged autocorrelation of RMM amplitude in the observations and the model, as well as the lead-lag correlation between RMM1 and RMM2. Both of these generally highlight that the models' RMM indices compare favorably to observations, though the RMM in three models (CESM, GISS, and GFDL) has an

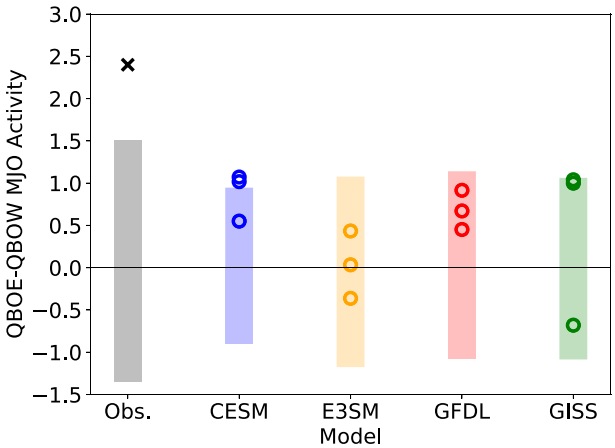

Figure 5. The change in December-February Madden-Julian oscillation (MJO) activity (measured by the standard deviation (in W/m^2) of 20–100 days filtered, eastward wavenumber 1–5 OLR over the warm pool (50°−170°E, 20°S–5°N), as in Kim et al. (2020)) between QBOE and QBOW. The shaded bar is the 2.5–97.5 percentile range of changes in MJO activity taken across bootstrapped periods in each model or in observations when the QBO was neutral. The observed change is denoted in the left-most column with a black "x."

amplitude autocorrelation that falls off faster than observed, suggesting a less persistent MJO. The lead-lag correlation is also fairly comparable, illustrating that the model MJO propagates approximately as coherently as observed. GFDL and CESM somewhat underestimate the degree of the correlation (i.e., the minima and maxima in Figure 4d) and the distance between the peaks is somewhat shorter, indicating slightly faster-than-observed MJO propagation in these two models. But overall, these diagnostics confirm that MJO representation via the RMM index in models is generally comparable to observations. Some models, such as E3SM, show even stronger MJO amplitude and compare quite favorably with observations.

3.3. The Lack of a QBO-MJO Connection

While QBO signals across the models are well-represented with nudging, and no clear systematic MJO bias appears via the metrics described above, none of the four models shows a clear QBO-MJO connection in any ensemble member, or in the ensemble mean. We illustrate this lack of a link through both changes in the MJO activity (as defined by the 20–100 days bandpass-filtered, eastward wavenumber 1–5 filtered OLR) and the correlation between the U50 and RMM indices.

We first examined changes in MJO activity during QBOE and QBOW winters (DJF). Figure 5 shows the difference in the standard deviation of filtered OLR over the Maritime continent region (50°−170°E, 20°S–5°N) between QBOE and QBOW: the strong increase in the standard deviation in observations (over 2 W/m^2, indicating enhanced subseasonal convective variability during QBOE periods) is not evident in the models. Some ensemble members show positive changes, but none are as strong as observations, and in the GISS and E3SM models, changes of both signs are found. Note that the observed values in Figure 5 (∼2.4 W/m^2) are slightly smaller than the values reported in Kim et al. (2020) (∼2.8 W/m^2, see their Figure 3); further analysis (not shown) reveals that this likely reflects our use of NOAA OLR, whereas ERA-I values were used in that study. Previous studies have also noted a discrepancy in moisture variance associated with the MJO among different reanalyses (Ren et al., 2021); more to the point, for both cases, the observed values are still significantly larger than in the models.

Further, we conducted a bootstrap analysis to sample changes in MJO activity over randomly selected winter periods when the nudged QBO was neutral (Kim et al., 2020), sampling equivalent numbers of QBOE and QBOW samples to what is found in each model. The bootstrap analysis generally produces larger or comparable magnitudes in MJO variance than the models' QBO-related signals (shaded bars in Figure 5), indicating that the simulated QBO signals here are indistinguishable from interannual variability unassociated with the QBO. Two ensemble members in CESM show slightly higher change than noise, though the relationship is still half of the observed and a third ensemble member does not show the same link.

Analysis of the correlation between U50 and RMM in the models also does not show a strong QBO-MJO connection. While the observed QBO-MJO link is evident only in winter, we explored the correlation throughout the year across all model simulations, since an explanation for why the observed link should appear only in DJF is not forthcoming and a strong model link in a season aside from winter would still be of interest. Figure 6 shows the correlation between 3-month mean RMM amplitude and U50 throughout the year. A dip which leads to significant anticorrelation in observations from November-January to January-March is evident, as other studies have shown (Marshall et al., 2017; Martin, Son, et al., 2021). Yet no model shows a seasonal modulation like that observed. One CESM and GISS ensemble member and two members of the GFDL model show limited periods of significant correlation or anticorrelation, but these are either of the wrong sign (GFDL), are over a limited period (CESM), or are much weaker than observed (GISS, GFDL, and CESM). As a few spurious correlations can be expected when analyzing over many ensemble members across many seasons, a few points of significance in the models are not surprising. Taken as a whole, it seems conclusive that no model shows a significant QBO-MJO link with a magnitude or characteristics comparable to that in observations. Ensemble means also show no link in any model.

It remains difficult to identify what explains the lack of a QBO-MJO connection in models. MJO biases, for example, the 3D structure of the MJO, have been noted as a possible source of error that stratospheric nudging

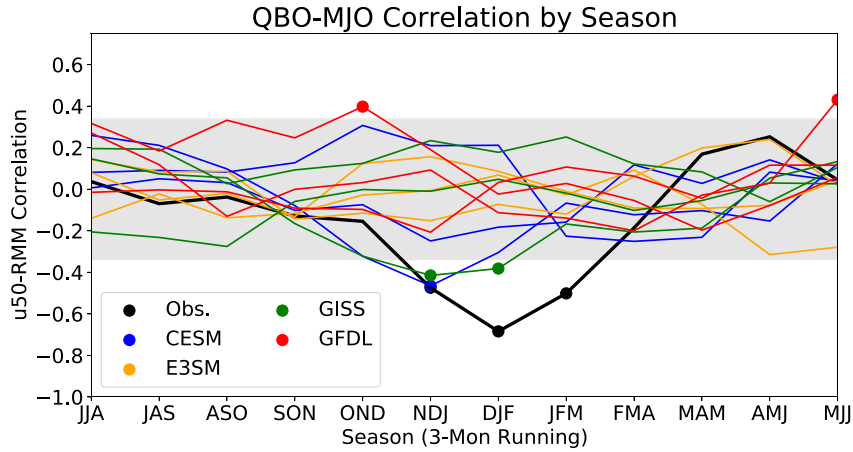

Figure 6. The correlation between the 3-month mean Real-time Multivariate Madden-Julian oscillation index (RMM) amplitude and U50 QBO index, with the months indicated across the *x* axis (beginning in June-August and ending May-July). Each ensemble member is shown separately. The gray shading denotes the 95% significance level using a *t* test; correlations that are significant above or below that level are denoted with a dot.

experiments do not resolve (M21). Yet absent a clear theoretical hypothesis for what drives the observed QBO-MJO interaction, pin-pointing model deficiencies is a challenge. M21 explored whether aliasing between the imposed QBO and different sea-surface temperature patterns showed any relationship to the QBO-MJO interaction, but found no clear signal.

Here we explore two other hypotheses recently presented in the literature (Sakaeda et al., 2020) regarding possible metrics or mechanisms that may be important for the QBO-MJO link: cloud-radiative feedbacks and the vertical structure of the MJO. While the nudging experiments conducted here do not correct tropospheric biases in either MJO cloud feedbacks or vertical structure, diagnosing these aspects of models may illuminate any issues and help further guide hypotheses of what drives the observed QBO-MJO interaction and their biases in models.

Our first hypothesis, following Sakaeda et al. (2020), is that the uniquely strong cloud-radiative feedback associated with the observed MJO may make it especially susceptible to modulation by the QBO. In particular, this may explain why only the MJO and no other tropical convectively coupled waves are modulated by the QBO (Abhik & Hendon, 2019; Sakaeda et al., 2020). We note that the change in MJO cloud-radiative feedback in different QBO phases in observations does not appear statistically significant (Sakaeda et al., 2020), making it unclear if cloud-radiative feedbacks are truly a central mechanism for the QBO-MJO link. Still, if models underestimated the strength of MJO cloud-radiative feedbacks, it could both help explain the lack of a model QBO-MJO link and support the hypothesized importance of this physical process.

We diagnose MJO-related cloud-radiative feedback using the greenhouse enhancement parameter (Adames & Kim, 2016; Kim et al., 2015; Sakaeda et al., 2020), which measures how much reduction in OLR occurs due to anomalous water vapor and cloudiness per unit of precipitation. A stronger reduction in OLR indicates a colder cloud top that is generally associated with deeper convection. Our specific methodology follows Adames and Kim (2016) and Sakaeda et al. (2020) by calculating the relationship between rainfall and OLR during DJF. We use 20–100 days bandpass-filtered OLR and rain anomalies at latitude-longitude points from 60°−180°E to 15°N–15°S, and due to availability of observed TRMM rainfall data, only the period 1998–2015 is used. To facilitate comparison the same time period is used in the models; model results are not sensitive to changing our analysis using all available years. Rainfall and OLR are binned every 2 W/m^2 for OLR and every 0.2 mm/hr for rain in Figure 7, and the slope of the regression line ("*r*" in Adames and Kim (2016)) represents the cloud-radiative feedback parameter. The slope of this line, which is negative, indicates how strongly long-wave radiative warming increases with rainfall.

Our observed value of *r* (−0.167) agrees very well with Adames and Kim (2016). Values of *r* across ensemble members show that the majority of models (CESM, GFDL, GISS) show slightly weaker MJO cloud feedbacks (higher *r* values; listed in the top right of each panel in Figure 7), while one model (E3SM) has *r* values across the ensemble that correspond well with observations. Further, in models with weaker cloud feedbacks, biases in

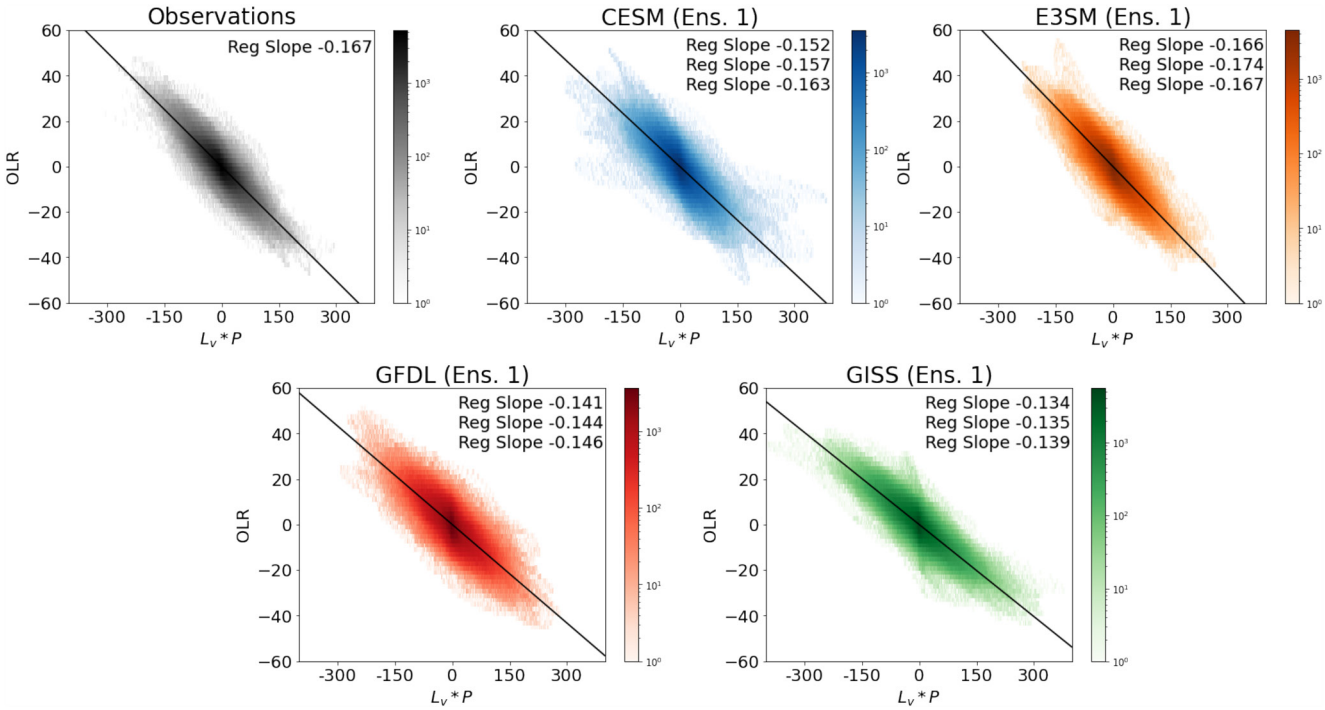

Figure 7. Shading shows the number density of 20–100 days bandpass-filtered rainfall (*x* axis; scaled by latent heat of vaporization) and long-wave radiation (OLR) (*y* axis) anomalies for 0.02 mm/hr and 2 W/m^2 sized bins. Panels are observations (top left) and the first ensemble member of each model (other panels). The black line is the regression coefficient between OLR and rainfall, which represents the cloud-radiative feedback parameter. The regression coefficient is listed in the top right; for the model runs, while only the first ensemble member is shown, the regression coefficient for all three members is listed.

r relative to observations are not large compared to the observed range between the MJO and other convectively coupled equatorial waves (e.g., Sakaeda et al., 2020; their Figure 14). This shows that the models capture values of MJO cloud feedback that appear only slightly weaker-than-observed, and coupled with the fact that cloud feedback in E3SM looks comparable to observations and the model has no QBO-MJO link, capturing the correct cloud feedback parameter is not enough to ensure a connection of the MJO to the QBO. This does not in and of itself prove cloud-radiative feedbacks are not central to the observed QBO-MJO link: more complex and subtle processes may be at play in observations, or other important processes may be missing from models. But at least by this metric, no major deficiency is evident systematically across the model experiments we conducted.

Further analysis of how the cloud feedback parameter varied in QBOE versus QBOW across the model showed a wide range of behavior. In observations, Sakaeda et al. (2020) noted a 6% increase in *r* in QBOE versus QBOW; while the change was not significant, they suggested stronger cloud-radiative feedbacks in QBOE may be linked to increased MJO activity in QBOE. We found no robust QBO-related change in *r* in model simulations: in all four models at least one ensemble member showed an increase of r in QBOE versus QBOW and at least one member showed a decrease, suggesting no systematic relationship between the imposed QBO and cloud-radiative feedbacks. The interpretation of this finding would depend on whether the observed connection between *r* and the QBO phase is indeed robust and at this point it is unclear whether that is the case (Sakaeda et al., 2020). If the observed connection is robust, then the fact that the models do not exhibit it could be a potential reason for their lack of QBO-MJO connection. However, if the connection between *r* and the QBO is not meaningful in observations, then the model results here are consistent with there not being a true connection. Thus, future work which examines how cloud feedbacks, the QBO, and the MJO interact in observations in more detail would be very useful.

A second hypothesis we examine is that biases in the vertical structure of the MJO—in particular the vertical velocity—may be important. Several studies have proposed that the MJO's vertical structure may be important in explaining why and how it is modulated by the QBO, either through the vertical structure of MJO temperature signals in the TTL (Hendon & Abhik, 2018) or through the vertical top-heaviness of MJO vertical velocity (Sakaeda et al., 2020).

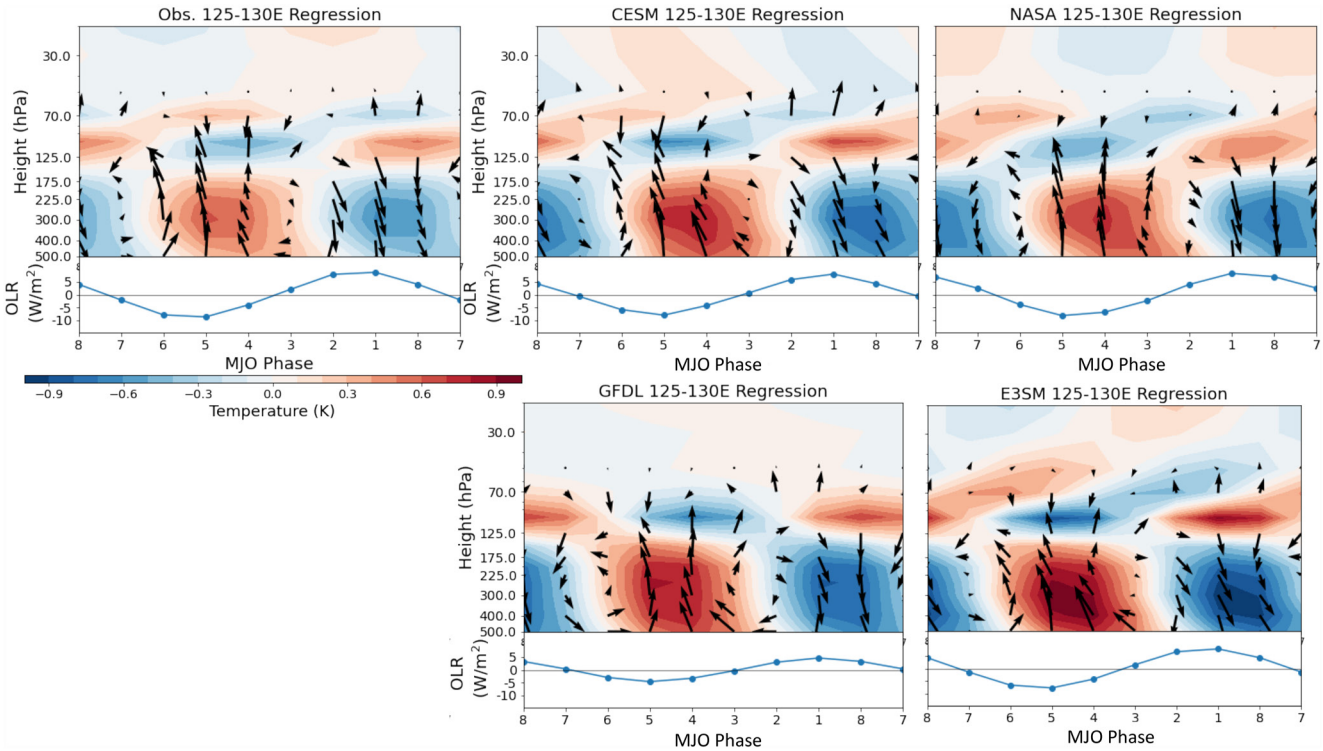

Figure 8. Regression plots of December-February (DJF) temperature, zonal wind, and vertical velocity as well as long-wave radiation (OLR) (bottom portion of each panel) regressed onto the Real-time Multivariate Madden-Julian oscillation index (RMM) index. Variables are averaged from 5°S to 5°N and from 125°E to 130°E, and the seasonal cycle is removed before regressing against RMM1–RMM2 (Phase 3/4), RMM1 (Phase 4/5), RMM1 + RMM2 (Phase 5/6), and RMM2 (Phase 6/7). Multiplying these values by negative one represents Madden-Julian oscillation (MJO) Phases 7/8 to 2/3. The regression coefficient is scaled by the standard deviation of each variable, and vertical velocity is multiplied by −1 (upward indicates ascent), and by 1,000 for ease of interpretation. The *y* axis is log pressure. MJO phases are shown in descending order so that eastward propagation is depicted from left to right.

We diagnose how well the models represent the MJO's vertical structure via a regression analysis focusing in particular on equatorial signals in vertical velocity, zonal wind, and temperature around the Maritime Continent region where the observed QBO-MJO link is strongest (Figure 3b). Figure 8 shows wind and temperature signals around the Maritime Continent regressed onto RMM phases 1–8 following the methodology described in Hendon and Abhik (2018) for ERA-5 reanalysis and the four models. This localized region, in which MJO activity is high and the MJO-QBO signal is pronounced (Kim et al., 2020, see their Figure 1), is chosen to ensure consistency with prior literature. Over this region, models show a range of vertical structures in temperature and wind that look generally quite similar to the observations (Figure 8). In particular, all models show TTL "cold caps" (Holloway & Neelin, 2007) above and slightly east of peak convection in MJO phases 4 and 5. The precise phasing and magnitude of model cold caps differ somewhat: the signal is slightly too weak in the GISS model (as noted in M21), but has comparable strength to reanalysis in the other three models. Most models also show upward propagation of Kelvin waves into the stratosphere emanating from the MJO (upward tilting warm and cold anomalies above ∼125 hPa), though this feature is not evident in the GFDL model.

While temperature and wind signals look comparable in Figure 8, we examined the model MJO vertical velocity in more detail, as Sakaeda et al. (2020) have pointed to the top-heaviness of MJO vertical velocity as possibly important for the observed QBO-MJO link. Again we focus on vertical velocity signals around the Maritime Continent where the observed QBO-MJO link is strongest. Figure 9 shows a similar regression plot to Figure 8, regressing vertical velocity against RMM1 (corresponding to the MJO Phase 4/5) and taking a slightly broader 120°−150°E region where strong convection during active MJO is evident. Comparison of reanalysis (ERA-5) and model vertical velocity (Figure 9) indicates that models tend to show vertical velocity profiles associated with the MJO around the MC that are either too bottom-heavy (E3SM, CESM, GISS), or too weak overall (GFDL). For bottom-heavy models, vertical velocity peaks in the upper troposphere around 600 hPa, whereas the observed peak tends to be between 400 and 500 hPa, consistent qualitatively with other studies (Inoue et al., 2020; Sakaeda

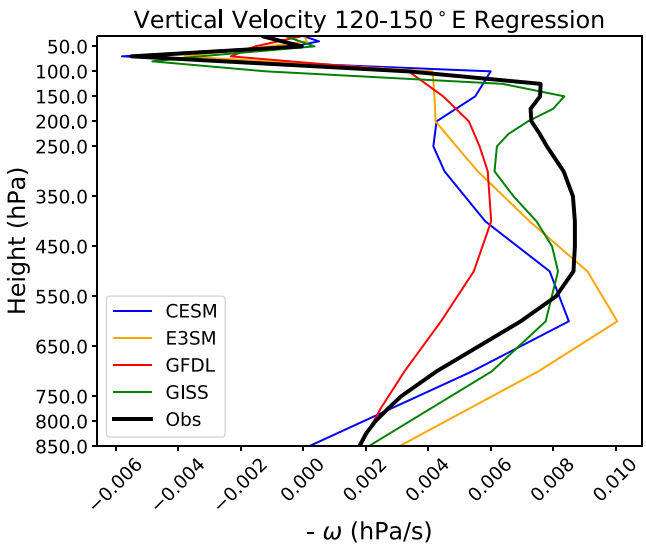

Figure 9. Regression plots of December-February (DJF) vertical velocity, similar to Figure 8, but for Madden-Julian oscillation (MJO) Phase 4/5 (e.g., regression onto RMM 1) averaged over 120°−150°E (e.g., capturing active MJO conditions over the Maritime Continent, and averaging over the region of deep convection and ascent).

et al., 2020). In the case of the GFDL model, the peak in vertical velocity is more comparable to the reanalysis but overall ascent is much weaker throughout the troposphere. Note that although Figure 9 only shows vertical velocities from ERA-5, Sakaeda et al. (2020) identified a strong top-heaviness of vertical motion associated with the MJO in two separate reanalysis products (ERA-I and JRA-55, Kobayashi et al., 2015). That said, care must be taken when quantitatively comparing against reanalysis vertical velocities, as these likely reflect large contributions from underlying model physics as well.

These caveats aside, the results shown in Figure 9 point to a potential common deficiency across models related to the vertical structure of the vertical velocity. Coupled with a weaker cloud-radiative feedback in some models, it is possible that this may in part contribute to the lack of a QBO-MJO link observed, though we note that E3SM shows a comparable cloud-radiative feedback to that observed and still did not possess a QBO-MJO link. This makes it difficult to point directly to biases in vertical velocity as the main culprit of the missing QBO-MJO link in models, but does suggest more work centered on understanding how vertical velocity profiles associated with MJO convection, and more generally the vertical structure of the MJO, may be connected to the QBO-MJO linkage would be valuable and possibly illuminating.

4. Discussion and Conclusions

The observed QBO-MJO connection—an increase in MJO activity in the easterly phase of QBO relative to the westerly phase—remains difficult to capture in free-running climate models. Building on previous work (M21), we carried out a series of experiments in which the stratosphere in four climate models was nudged toward reanalysis, imposing QBO signals while allowing the troposphere to freely evolve. The four state-of-the-art climate models were run from 1980 to 2015, with three ensemble members per simulation, nudged toward reanalysis during that period. Despite very good representation of the key aspects of the QBO, including wind and temperature signals, we find that no model exhibits a QBO-MJO connection that is comparable to that in observations.

In examining the possible cause of why models show no QBO-MJO link, we explored model representation of the MJO, including the vertical structure of the MJO around the Maritime Continent, and cloud-radiative feedbacks associated with the observed versus modeled MJO. Too-weak cloud-radiative feedbacks were one hypothesized reason for the lack of the QBO-MJO link, but that does not appear to be the case overall: MJO-related cloud-radiative feedbacks were somewhat weaker than observed in most models, but one (E3SM) showed values consistent with observations and still failed to show a QBO-MJO link. This does not mean that clouds are not central to the observed link, but highlights the need for more specific and testable hypotheses. In particular, we noted that while the observed MJO cloud-radiative feedbacks strengthened slightly during QBOE, models do not simulate this change. Whether this indicates that the observed change is not significant (as was found in Sakaeda et al. (2020)) or that the models miss an important process remains unresolved.

We showed that models have vertical structures of wind and temperature that are largely consistent with observations, including finding that all models represent a cold cap above active MJO convection. However, model vertical velocity appears either weaker or more bottom-heavy than observed. Sakaeda et al. (2020) identified the top-heavy nature of MJO vertical velocity as possibly important for explaining features of the observed QBO-MJO connection, like why it manifests only in winter, while other convectively coupled waves are not affected (Abhik & Hendon, 2019; Sakaeda et al., 2020), and why an observed QBO-MJO link does not appear to have existed prior to ∼1980 (Klotzbach et al., 2019). A specific hypothesis regarding how the MJO's vertical structure may link the QBO and MJO is still lacking however, and future work examining this aspect of the QBO-MJO link may also be fruitful.

Overall, however, it remains possible that a host of other model biases or processes could contribute to the lack of a QBO-MJO connection. The results here, coupled with findings in M21 using a larger ensemble in a single

model, strongly suggest that nudging of the QBO winds in conventional climate models is not sufficient to capture a QBO-MJO connection. This implies that stratospheric biases in the zonal wind or the temperature of the tropics of climate models is not the reason, or at least not the only reason, why models fail to simulate the QBO-MJO connection. Stratospheric biases still exist with nudging however; as we noted, the divergent TEM circulation in the stratosphere for example, is much less constrained with nudging. It is not clear whether this is important for the QBO-MJO link, but continuing to examine other stratospheric biases in models as they relate to the MJO may help guide future modeling strategies. In particular, one contributor to differences among the models might relate to the use of interactive ozone schemes, wherein local temperatures are modified by prognostic stratospheric ozone through changes in solar heating. Though beyond the scope of this study, recent work has highlighted the importance of ozone feedbacks on QBO structure (DallaSanta et al., 2021) and future work should examine whether this may influence QBO-MJO modulation in models.

In addition to stratospheric biases, tropospheric biases may be important, especially as they relate to the MJO, or having an interactive stratosphere rather than a nudged one may be central for capturing the QBO-MJO connection through improved representation of the QBO descent into the lowermost stratosphere (Butchart et al., 2003; DallaSanta et al., 2021), while also not limiting wave-mean flow interactions. We recommend future approaches or modeling experiments in particular to look at different modeling frameworks, perhaps at higher resolution using super-parameterization.

Finally, we emphasize that the data set here offers a unique suite of experiments in which to examine other questions related to downward stratospheric impacts in climate models, not limited to those in the tropics. Future work leveraging the output from these model experiments may therefore be of interest to the broader stratosphere-troposphere community.

Data Availability Statement

All observational and reanalysis data sets used in this study are publicly available. The RMM index is available at http://www.bom.gov.au/climate/mjo/. For reanalysis and observed data, NOAA Interpolated OLR (Liebmann & Smith, 1996) is available at https://psl.noaa.gov/data/gridded/data.olrcdr.interp.html; ERA-5 reanalysis (Hersbach et al. (2020)) is available at https://cds.climate.copernicus.eu/#!/search?text=ERA5&type=dataset. TRMM data are available from https://disc.gsfc.nasa.gov/datasets/TRMM_3B42_Daily_7/summary. Data from the modeling experiments used in the figures and analysis in this study is available at https://doi.org/10.5281/zenodo.7647503.

Acknowledgments
ZM acknowledges support from the National Science Foundation under Award 2020305. This work was supported by the National Center for Atmospheric Research, which is a major facility sponsored by the National Science Foundation (NSF) under Cooperative Agreement 1852977. The CESM simulations were run with NCAR Community Computing on the Computational and Information Systems Laboratory's Cheyenne system (doi: https://doi.org/10.5065/D6RX99HX). Portions of this study were supported by the Regional and Global Model Analysis (RGMA) component of the Earth and Environmental System Modeling Program of the U.S. Department of Energy's Office of Biological and Environmental Research (BER) via National Science Foundation IA 1947282, and under Award Number DE-SC0022070. The E3SM simulations were supported by the Energy Exascale Earth System Model (E3SM) project, funded by the DOE BER through the Earth System Model Development program area using computing resources provided by the National Energy Research Scientific Computing Center (NERSC), a DOE Office of Science User Facility supported by the Office of Science of DOE under contract DE-AC02-05CH11231. The Pacific Northwest National Laboratory (PNNL) is operated for DOE by Battelle Memorial Institute under contract DE-AC05-76RL01830. Work at Lawrence Livermore National Laboratory (LLNL) was performed under the auspices of the U.S. DOE by LLNL under contract No. DE-AC52-07NA27344. Support has also been received from the LLNL LDRD project 22-ERD-008, "Multiscale Wildfire Simulation Framework and Remote Sensing." PL is supported under award NA18OAR4320123 from the National Oceanic and Atmospheric Administration, U.S. Department of Commerce. The statements, findings, conclusions, and recommendations are those of the author(s) and do not necessarily reflect the views of the National Oceanic and Atmospheric Administration, or the U.S. Department of Commerce. We acknowledge GFDL resources made available for this research. Climate modeling at GISS is supported by the NASA Modeling, Analysis and Prediction program, and resources supporting this work were provided by the NASA High-End Computing (HEC) Program through the NASA Center for Climate Simulation (NCCS) at Goddard Space Flight Center. HK was supported by the NSF Grant AGS-1652289 and Korean Meteorological Administration (KMA) R&D Program Grant KMI2021-01210.

References

Abhik, S., & Hendon, H. H. (2019). Influence of the QBO on the MJO during coupled model multiweek forecasts. *Geophysical Research Letters*, *46*, 9213–9221. https://doi.org/10.1029/2019GL083152

Adames, Á. F., & Kim, D. (2016). The MJO as a dispersive, convectively coupled moisture wave: Theory and observations. *Journal of the Atmospheric Sciences*, *73*(3), 913–941. https://doi.org/10.1175/jas-d-15-0170.1

Ahn, M.-S., Kim, D., Kang, D., Lee, J., Sperber, K. R., Gleckler, P. J., et al. (2020). MJO propagation across the maritime continent: Are CMIP6 models better than CMIP5 models? *Geophysical Research Letters*, *47*, e2020GL087250. https://doi.org/10.1029/2020GL087250

Andrews, D. G., Holton, J. R., & Leovy, C. B. (1987). *Middle atmosphere dynamics* (No. 40). Academic Press.

Anstey, J. A., Simpson, I. R., Richter, J. H., Naoe, H., Taguchi, M., Serva, F., et al. (2022). Teleconnections of the quasi-biennial oscillation in a multi-model ensemble of qbo-resolving models. *Quarterly Journal of the Royal Meteorological Society*, *148*(744), 1568–1592. https://doi.org/10.1002/qj.4048

Back, S.-Y., Han, J.-Y., & Son, S.-W. (2020). Modeling evidence of QBO-MJO connection: A case study. *Geophysical Research Letters*, *47*, e2020GL089480. https://doi.org/10.1029/2020GL089480

Baldwin, M., Gray, L., Dunkerton, T., Hamilton, K., Haynes, P., Randel, W. J., et al. (2001). The quasi-biennial oscillation. *Reviews of Geophysics*, *39*(2), 179–229. https://doi.org/10.1029/1999RG000073

Butchart, N., Scaife, A. A., Austin, J., Hare, S. H., & Knight, J. R. (2003). Quasi-biennial oscillation in ozone in a coupled chemistry-climate model. *Journal of Geophysical Research*, *108*(D15), 4486. https://doi.org/10.1029/2002JD003004

Camargo, S. J., & Sobel, A. H. (2010). Revisiting the influence of the quasi-biennial oscillation on tropical cyclone activity. *Journal of Climate*, *23*(21), 5810–5825. https://doi.org/10.1175/2010JCLI3575.1

Chrysanthou, A., Maycock, A. C., Chipperfield, M. P., Dhomse, S., Garny, H., Kinnison, D., et al. (2019). The effect of atmospheric nudging on the stratospheric residual circulation in chemistry-climate models. *Atmospheric Chemistry and Physics*, *19*(17), 11559–11586. https://doi.org/10.5194/acp-19-11559-2019

DallaSanta, K., Orbe, C., Rind, D., Nazarenko, L., & Jonas, J. (2021). Dynamical and trace gas responses of the quasi-biennial oscillation to increased CO_2. *Journal of Geophysical Research: Atmospheres*, *126*, e2020JD034151. https://doi.org/10.1029/2020JD034151

Danabasoglu, G., Lamarque, J.-F., Bacmeister, J., Bailey, D., DuVivier, A., Edwards, J., et al. (2020). The community earth system model version 2 (CESM2). *Journal of Advances in Modeling Earth Systems*, *12*, e2019MS001916. https://doi.org/10.1029/2019MS001916

Davis, N. A., Callaghan, P., Simpson, I. R., & Tilmes, S. (2022). Specified dynamics scheme impacts on wave-mean flow dynamics, convection, and tracer transport in CESM2 (WACCM6). *Atmospheric Chemistry and Physics*, *22*(1), 197–214. https://doi.org/10.5194/acp-22-197-2022

Dee, D. P., Uppala, S. M., Simmons, A. J., Berrisford, P., Poli, P., Kobayashi, S., et al. (2011). The ERA-interim reanalysis: Configuration and performance of the data assimilation system. *Quarterly Journal of the Royal Meteorological Society*, *137*(656), 553–597. https://doi.org/10.1002/qj.828

DeWeaver, E., & Nigam, S. (1997). Dynamics of zonal-mean flow assimilation and implications for winter circulation anomalies. *Journal of the Atmospheric Sciences*, *54*(13), 1758–1775. https://doi.org/10.1175/1520-0469(1997)054<1758:DOZMFA>2.0.CO;2

Douville, H. (2009). Stratospheric polar vortex influence on Northern Hemisphere winter climate variability. *Geophysical Research Letters*, *36*, L18703. https://doi.org/10.1029/2009GL039334

Ebdon, R. (1960). Notes on the wind flow at 50 mb in tropical and sub-tropical regions in January 1957 and January 1958. *Quarterly Journal of the Royal Meteorological Society*, *86*(370), 540–542. https://doi.org/10.1002/qj.49708637011

Eyring, V., Bony, S., Meehl, G. A., Senior, C. A., Stevens, B., Stouffer, R. J., & Taylor, K. E. (2016). Overview of the coupled model intercomparison project phase 6 (CMIP6) experimental design and organization. *Geoscientific Model Development*, *9*(5), 1937–1958. https://doi.org/10.5194/gmd-9-1937-2016

Feng, P.-N., & Lin, H. (2019). Modulation of the MJO-related teleconnections by the QBO. *Journal of Geophysical Research: Atmospheres*, *124*, 12022–12033. https://doi.org/10.1029/2019JD030878

Ferranti, L., Palmer, T., Molteni, F., & Klinker, E. (1990). Tropical-extratropical interaction associated with the 30–60 day oscillation and its impact on medium and extended range prediction. *Journal of the Atmospheric Sciences*, *47*(18), 2177–2199. https://doi.org/10.1175/1520-0469(1990)047<2177:TEIAWT>2.0.CO;2

Garfinkel, C. I., & Hartmann, D. L. (2011). The influence of the quasi-biennial oscillation on the troposphere in winter in a hierarchy of models. Part II: Perpetual winter WACCM runs. *Journal of the Atmospheric Sciences*, *68*(9), 2026–2041. https://doi.org/10.1175/2011JAS3702.1

Gelaro, R., McCarty, W., Suárez, M. J., Todling, R., Molod, A., Takacs, L., et al. (2017). The modern-era retrospective analysis for research and applications, version 2 (MERRA-2). *Journal of Climate*, *30*(14), 5419–5454. https://doi.org/10.1175/JCLI-D-16-0758.1

Gerber, E. P., & Manzini, E. (2016). The dynamics and variability model intercomparison project (DynVarMIP) for CMIP6: Assessing the stratosphere–troposphere system. *Geoscientific Model Development*, *9*(9), 3413–3425. https://doi.org/10.5194/gmd-9-3413-2016

Golaz, J.-C., Caldwell, P. M., Van Roekel, L. P., Petersen, M. R., Tang, Q., Wolfe, J. D., et al. (2019). The DOE E3SM coupled model version 1: Overview and evaluation at standard resolution. *Journal of Advances in Modeling Earth Systems*, *11*, 2089–2129. https://doi.org/10.1029/2018MS001603

Gray, L. J., Anstey, J. A., Kawatani, Y., Lu, H., Osprey, S., & Schenzinger, V. (2018). Surface impacts of the quasi biennial oscillation. *Atmospheric Chemistry and Physics*, *18*(11), 8227–8247. https://doi.org/10.5194/acp-18-8227-2018

Held, I., Guo, H., Adcroft, A., Dunne, J., Horowitz, L., Krasting, J., et al. (2019). Structure and performance of GFDL's CM4. 0 climate model. *Journal of Advances in Modeling Earth Systems*, *11*, 3691–3727. https://doi.org/10.1029/2019MS001829

Hendon, H. H., & Abhik, S. (2018). Differences in vertical structure of the Madden-Julian Oscillation associated with the quasi-biennial oscillation. *Geophysical Research Letters*, *45*, 4419–4428. https://doi.org/10.1029/2018GL077207

Hersbach, H., Bell, B., Berrisford, P., Hirahara, S., Horányi, A., Muñoz-Sabater, J., et al. (2020). The ERA5 global reanalysis [Dataset]. Quarterly Journal of the Royal Meteorological Society, *146*, 1999–2049. https://doi.org/10.1002/qj.3803.730

Hitchcock, P., & Haynes, P. H. (2014). Zonally symmetric adjustment in the presence of artificial relaxation. *Journal of the Atmospheric Sciences*, *71*(11), 4349–4368. https://doi.org/10.1175/JAS-D-14-0013.1

Hitchcock, P., & Simpson, I. R. (2014). The downward influence of stratospheric sudden warmings. *Journal of the Atmospheric Sciences*, *71*(10), 3856–3876. https://doi.org/10.1175/JAS-D-14-0012.1

Holloway, C. E., & Neelin, J. D. (2007). The convective cold top and quasi equilibrium. *Journal of the Atmospheric Sciences*, *64*(5), 1467–1487. https://doi.org/10.1175/JAS3907.1

Holton, J. R., & Tan, H.-C. (1980). The influence of the equatorial quasi-biennial oscillation on the global circulation at 50 mb. *Journal of the Atmospheric Sciences*, *37*(10), 2200–2208. https://doi.org/10.1175/1520-0469(1980)037<2200:TIOTEQ>2.0.CO;2

Hsu, J., & Prather, M. J. (2009). Stratospheric variability and tropospheric ozone. *Journal of Geophysical Research*, *114*, D06102. https://doi.org/10.1029/2008JD010942

Inoue, K., Adames, Á. F., & Yasunaga, K. (2020). Vertical velocity profiles in convectively coupled equatorial waves and MJO: New diagnoses of vertical velocity profiles in the wavenumber-frequency domain. *Journal of the Atmospheric Sciences*, *77*(6), 2139–2162. https://doi.org/10.1175/JAS-D-19-0209.1

Jeuken, A., Siegmund, P., Heijboer, L., Feichter, J., & Bengtsson, L. (1996). On the potential of assimilating meteorological analyses in a global climate model for the purpose of model validation. *Journal of Geophysical Research*, *101*(D12), 16939–16950. https://doi.org/10.1029/96JD01218

Kelley, M., Schmidt, G. A., Nazarenko, L. S., Bauer, S. E., Ruedy, R., Russell, G. L., et al. (2020). GISS-E2. 1: Configurations and climatology. *Journal of Advances in Modeling Earth Systems*, *12*, e2019MS002025. https://doi.org/10.1029/2019MS002025

Kiladis, G. N., Dias, J., Straub, K. H., Wheeler, M. C., Tulich, S. N., Kikuchi, K., et al. (2014). A comparison of OLR and circulation-based indices for tracking the MJO. *Monthly Weather Review*, *142*(5), 1697–1715. https://doi.org/10.1175/MWR-D-13-00301.1

Kim, D., Ahn, M.-S., Kang, I.-S., & Del Genio, A. D. (2015). Role of longwave cloud-radiation feedback in the simulation of the Madden-Julian oscillation. *Journal of Climate*, *28*(17), 6979–6994. https://doi.org/10.1175/JCLI-D-14-00767.1

Kim, D., Kang, D., Ahn, M.-S., DeMott, C., Hsu, C.-W., Yoo, C., et al. (2022). The Madden-Julian oscillation in the energy Exascale earth system model version 1. *Journal of Advances in Modeling Earth Systems*, *14*, e2021MS002842. https://doi.org/10.1029/2021MS002842

Kim, H., Caron, J. M., Richter, J. H., & Simpson, I. R. (2020). The lack of QBO-MJO connection in CMIP6 models. *Geophysical Research Letters*, *47*, e2020GL087295. https://doi.org/10.1029/2020GL087295

Kim, H., Richter, J. H., & Martin, Z. (2019). Insignificant QBO-MJO prediction skill relationship in the SubX and S2S subseasonal reforecasts. *Journal of Geophysical Research: Atmospheres*, *124*, 12655–12666. https://doi.org/10.1029/2019JD031416

Klotzbach, P., Abhik, S., Hendon, H., Bell, M., Lucas, C., Marshall, A. G., & Oliver, E. (2019). On the emerging relationship between the stratospheric quasi-biennial oscillation and the Madden-Julian oscillation. *Scientific Reports*, *9*(1), 2981. https://doi.org/10.1038/s41598-019-40034-6

Kobayashi, S., Ota, Y., Harada, Y., Ebita, A., Moriya, M., Onoda, H., et al. (2015). The jra-55 reanalysis: General specifications and basic characteristics. *Journal of the Meteorological Society of Japan Series II*, *93*(1), 5–48. https://doi.org/10.2151/jmsj.2015-001

Lee, J. C., & Klingaman, N. P. (2018). The effect of the quasi-biennial oscillation on the Madden-Julian oscillation in the Met Office Unified model global ocean mixed layer configuration. *Atmospheric Science Letters*, *19*(5), e816. https://doi.org/10.1002/asl.816

Liebmann, B., & Smith, C. A. (1996). Description of a complete (interpolated) outgoing longwave radiation dataset [Dataset]. *Bulletin of the American Meteorological Society*, *77*(6), 1275–1277. Retrieved from https://psl.noaa.gov/data/gridded/data.olrcdr.interp.html

Lim, Y., & Son, S.-W. (2020). QBO-MJO connection in CMIP5 models. *Journal of Geophysical Research: Atmospheres*, *125*, e2019JD032157. https://doi.org/10.1029/2019JD032157

Lim, Y., Son, S.-W., Marshall, A. G., Hendon, H. H., & Seo, K.-H. (2019). Influence of the QBO on MJO prediction skill in the subseasonal-to-seasonal prediction models. *Climate Dynamics*, *53*(3–4), 1681–1695. https://doi.org/10.1007/s00382-019-04719-y

Liu, Z., Ostrenga, D., Teng, W., & Kempler, S. (2012). Tropical Rainfall Measuring Mission (TRMM) precipitation data and services for research and applications. *Bulletin of the American Meteorological Society*, *93*(9), 1317–1325. https://doi.org/10.1175/BAMS-D-11-00152.1

Madden, R. A., & Julian, P. R. (1971). Detection of a 40–50 day oscillation in the zonal wind in the tropical pacific. *Journal of the Atmospheric Sciences*, *28*(5), 702–708. https://doi.org/10.1175/1520-0469(1971)028<0702:DOADOI>2.0.CO;2

Madden, R. A., & Julian, P. R. (1972). Description of global-scale circulation cells in the tropics with a 40–50 day period. *Journal of the Atmospheric Sciences*, *29*(6), 1109–1123. https://doi.org/10.1175/1520-0469(1972)029<1109:DOGSCC>2.0.CO;2

Marshall, A. G., Hendon, H. H., Son, S.-W., & Lim, Y. (2017). Impact of the quasi-biennial oscillation on predictability of the Madden-Julian oscillation. *Climate Dynamics*, *49*(4), 1365–1377. https://doi.org/10.1007/s00382-016-3392-0

Martin, Z., Orbe, C., Wang, S., & Sobel, A. (2021). The MJO-QBO relationship in a GCM with stratospheric nudging. *Journal of Climate*, *34*(11), 4603–4624. https://doi.org/10.1175/JCLI-D-20-0636.1

Martin, Z., Son, S.-W., Butler, A., Hendon, H., Kim, H., Sobel, A., et al. (2021). The influence of the quasi-biennial oscillation on the Madden-Julian oscillation. *Nature Reviews Earth & Environment*, *2*(7), 477–489. https://doi.org/10.1038/s43017-021-00173-9

Martin, Z., Vitart, F., Wang, S., & Sobel, A. (2020). The impact of the stratosphere on the MJO in a forecast model. *Journal of Geophysical Research: Atmospheres*, *125*, e2019JD032106. https://doi.org/10.1029/2019JD032106

Martin, Z., Wang, S., Nie, J., & Sobel, A. (2019). The impact of the QBO on MJO convection in cloud-resolving simulations. *Journal of the Atmospheric Sciences*, *76*(3), 669–688. https://doi.org/10.1175/JAS-D-18-0179.1

Mayer, K. J., & Barnes, E. A. (2020). Subseasonal midlatitude prediction skill following quasi-biennial oscillation and Madden-Julian Oscillation activity. *Weather and Climate Dynamics*, *1*(1), 247–259. https://doi.org/10.5194/wcd-1-247-2020

Orbe, C., Plummer, D. A., Waugh, D. W., Yang, H., Jöckel, P., Kinnison, D. E., et al. (2020). Description and evaluation of the specified-dynamics experiment in the chemistry-climate model Initiative. *Atmospheric Chemistry and Physics*, *20*(6), 3809–3840.

Orbe, C., Van Roekel, L., Adames, Á. F., Dezfuli, A., Fasullo, J., Gleckler, P. J., et al. (2020). Representation of modes of variability in six US climate models. *Journal of Climate*, *33*(17), 7591–7617. https://doi.org/10.1175/JCLI-D-19-0956.1

Reed, R. J., Campbell, W. J., Rasmussen, L. A., & Rogers, D. G. (1961). Evidence of a downward-propagating, annual wind reversal in the equatorial stratosphere. *Journal of Geophysical Research*, *66*(3), 813–818. https://doi.org/10.1029/JZ066i003p00813

Ren, P., Kim, D., Ahn, M.-S., Kang, D., & Ren, H.-L. (2021). Intercomparison of MJO column moist static energy and water vapor budget among six modern reanalysis products. *Journal of Climate*, *34*(8), 2977–3001. https://doi.org/10.1175/JCLI-D-20-0653.1

Richter, J. H., Anstey, J. A., Butchart, N., Kawatani, Y., Meehl, G. A., Osprey, S., & Simpson, I. R. (2020). Progress in simulating the quasi-biennial oscillation in CMIP models. *Journal of Geophysical Research: Atmospheres*, *125*, e2019JD032362. https://doi.org/10.1029/2019JD032362

Sakaeda, N., Dias, J., & Kiladis, G. N. (2020). The unique characteristics and potential mechanisms of the MJO-QBO relationship. *Journal of Geophysical Research: Atmospheres*, *125*, e2020JD033196. https://doi.org/10.1029/2020JD033196

Simpson, I., Hitchcock, P., Shepherd, T., & Scinocca, J. (2011). Stratospheric variability and tropospheric annular-mode timescales. *Geophysical Research Letters*, *38*, L20806. https://doi.org/10.1029/2011GL049304

Son, S.-W., Lim, Y., Yoo, C., Hendon, H. H., & Kim, J. (2017). Stratospheric control of the Madden-Julian oscillation. *Journal of Climate*, *30*(6), 1909–1922. https://doi.org/10.1175/JCLI-D-16-0620.1

Straub, K. H. (2013). MJO initiation in the real-time multivariate MJO index. *Journal of Climate*, *26*(4), 1130–1151. https://doi.org/10.1175/JCLI-D-12-00074.1

Tang, Q., Prather, M., & Hsu, J. (2011). Stratosphere-troposphere exchange ozone flux related to deep convection. *Geophysical Research Letters*, *38*, L03806. https://doi.org/10.1029/2010GL046039

Toms, B. A., Barnes, E. A., Maloney, E. D., & van den Heever, S. C. (2020). The global teleconnection signature of the Madden-Julian Oscillation and its modulation by the quasi-biennial oscillation. *Journal of Geophysical Research: Atmospheres*, *125*, e2020JD032653. https://doi.org/10.1029/2020JD032653

Ventrice, M. J., Wheeler, M. C., Hendon, H. H., Schreck, C. J., Thorncroft, C. D., & Kiladis, G. N. (2013). A modified multivariate Madden-Julian oscillation index using velocity potential. *Monthly Weather Review*, *141*(12), 4197–4210. https://doi.org/10.1175/MWR-D-12-00327.1

Wang, J., Kim, H.-M., Chang, E. K., & Son, S.-W. (2018). Modulation of the MJO and North Pacific storm track relationship by the QBO. *Journal of Geophysical Research: Atmospheres*, *123*, 3976–3992. https://doi.org/10.1029/2017JD027977

Wang, S., Tippett, M. K., Sobel, A. H., Martin, Z. K., & Vitart, F. (2019). Impact of the QBO on prediction and predictability of the MJO convection. *Journal of Geophysical Research: Atmospheres*, *124*, 11766–11782. https://doi.org/10.1029/2019JD030575

Wheeler, M. C., & Hendon, H. H. (2004). An all-season real-time multivariate MJO index: Development of an index for monitoring and prediction. *Monthly Weather Review*, *132*(8), 1917–1932. https://doi.org/10.1175/1520-0493(2004)132<1917:AARMMI>2.0.CO;2

Yoo, C., & Son, S.-W. (2016). Modulation of the boreal wintertime Madden-Julian oscillation by the stratospheric quasi-biennial oscillation. *Geophysical Research Letters*, *43*, 1392–1398. https://doi.org/10.1002/2016GL067762

Zhao, M., Golaz, J.-C., Held, I., Guo, H., Balaji, V., Benson, R., et al. (2018). The GFDL global atmosphere and land model AM4. 0/LM4. 0: 1. Simulation characteristics with prescribed SSTs. *Journal of Advances in Modeling Earth Systems*, *10*, 691–734. https://doi.org/10.1002/2017MS001208